

MIRROR SUPPORT DESIGN ISSUES RELATED TO THE METROLOGY MOUNT USED DURING PRIMARY MIRROR TESTING AT REOSC OPTIQUE

Larry Stepp, 6/13/94

I. Introduction

A number of questions about the design of the primary mirror support system have been raised at the Primary Mirror Assembly PDR and also with regard to the metrology mount used to test the mirrors during figuring at REOSC Optique. REOSC proposed that the Gemini primary mirrors could be tested on a metrology mount designed to match the ESO VLT mirror support, in order to save money. However, the Gemini Project staff are convinced that the metrology mount should match the mirror cell. If the mirrors were tested on a metrology mount different in configuration from the telescope mirror cell, the global figure might be adequately evaluated, but the local support print-through effects could only be inferred from analysis, leaving uncertainty about high-frequency errors that could jeopardize the telescope performance at short wavelengths. This issue is discussed further in Attachment A.

The PDR Committee shared the project's concern about the metrology mount. They stated in their report,

"The project should ensure that acceptance testing of the primary mirror on the polisher's premises occurs on a support fully representative of the operating conditions in the telescope."

However, in making the metrology mount match the mirror cell, there remains the question whether the metrology mount should change, or the mirror cell should change. Should the project adopt some or all of the aspects of the ESO support design?

To allow more time for analysis, and to enable the project to discuss the design issues openly without jeopardizing contract negotiations, the REOSC contract was written with three fixed-price options providing for:

1. Conversion of the REOSC metrology mount to a configuration matching the Gemini axial support design, having 120 support mechanisms arranged in five rings.
2. Addition of an air pressure support system (using edge seals provided by Gemini).
3. Addition of 72 active actuators around the edge of the mirror.

This report describes studies that were undertaken to answer questions about changing the Gemini design to more closely match the ESO design, in particular as the questions relate to the three metrology mount options listed above.

II. Technical Issues

The following technical issues must be addressed:

1. Should the Gemini pattern of 120 supports be changed to match the ESO pattern of 150 supports?
2. Should the support forces be oriented normal to the mirror surface, or parallel to the optical axis?

3. Should the air pressure support be used to minimize print-through, or should load spreaders be used?
4. Are the active optics actuators at the outer edge required?

These issues are covered in the following sections.

III. Number and Pattern of Axial Supports

The ESO VLT primary mirrors are very similar to the Gemini primary mirrors, having the same paraxial radius of curvature and about the same weight. However, the inside and outside diameters are slightly different:

Project	Inside Diameter	Outside Diameter
Gemini	1.18 m	8.1 m
VLT	1.00 m	8.2 m

Because the diameters of the VLT support rings are not optimized for the Gemini mirror dimensions, a Gemini mirror placed on the VLT support would need different support forces in each ring, as listed in Table 1.

Table 1. Support forces required to support the Gemini primary mirror on the ESO VLT support pattern, with minimum figure error.

Ring number	Force (N)
1	1210
2	1630
3	1440
4	1560
5	1500
6	1400

If these forces were applied to the Gemini mirror, the print-through would be at about the same level as the Gemini support design, about 10 nm RMS. However, to achieve these forces using a hydraulic whiffletree would require six different sizes of rolling diaphragms, some of which would be custom sizes. The interchangeability of the support mechanisms would be lost.

Further difficulties arise from the locations of the supports in the ESO design. The VLT support pattern cannot be evenly divided into six zones. This is illustrated in Figure 1. The Gemini support is designed to allow a six-zone mode of operation, in which a slight overconstraint in the axial support reduces the susceptibility to wind buffeting and to force errors by a factor of four. There would be practical difficulties in implementing this approach if the ESO support pattern were used, since it would have supports on the boundary lines between zones, and a hydraulic support cannot be half in one zone and half in another. There is no way to divide the ESO pattern into six zones with either left-right or 60° symmetry.

Another concern about the ESO VLT support pattern is that the supports are arranged in six rings instead of five as in the Gemini design. To maintain high stiffness for the entire support system, the Gemini design locates the axial supports directly above circumferential ribs in the mirror cell structure (see Figure 2). With five rings of supports, there is sufficient space between ribs to allow personnel access for maintenance. With six rings of supports, personnel access would be much more difficult, unless the entire concept of rigidly backing the axial supports with steel ribs was abandoned.

A final factor is cost. The cost of 150 support mechanisms with associated electronics, piping, etc., will be approximately 25% higher than the cost of 120. This difference could be more than \$200,000.

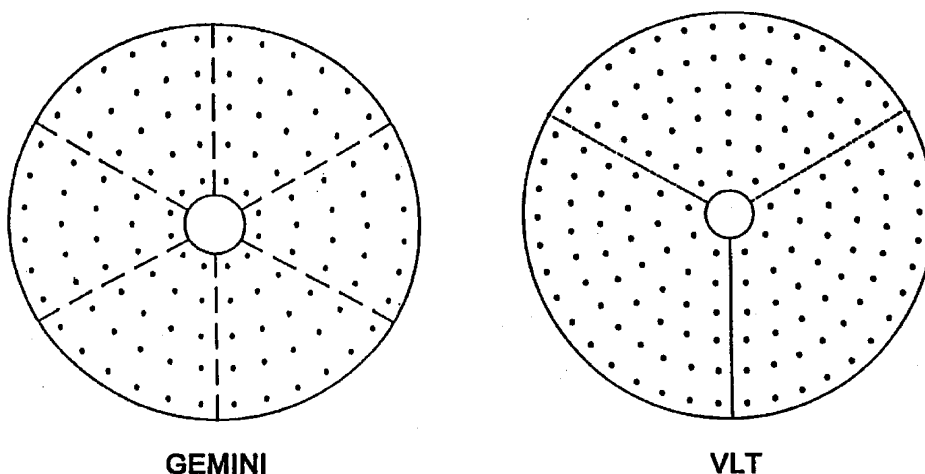


Figure 1. A comparison of support locations in the Gemini and ESO VLT axial support designs.

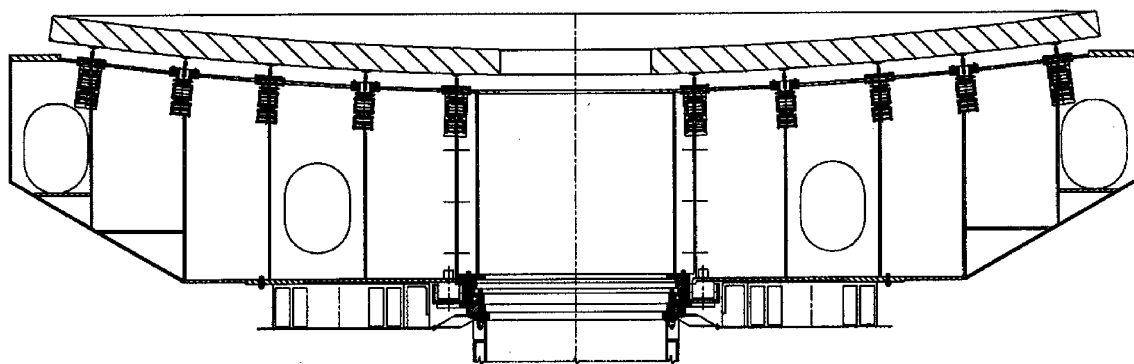


Figure 2. A cross section through the Gemini primary mirror cell.

IV. Support Force Orientation Normal or Parallel

In the Gemini support system design the axial supports act normal to the mirror back surface and the lateral supports act tangent to the curve. The VLT axial support mechanisms act parallel to the optical axis (although each force is split into three components by the load spreader). The Primary Mirror Assembly PDR Committee recommended,

"The tradeoffs between the "axial" supports being parallel to the optical axis instead of being normal to the mirror surface require investigation."

This issue could have a significant effect on the REOSC metrology mount, because the use of forces acting parallel to the optical axis would require Invar pads to be bonded to the back of the mirror, as ESO has done.

Earl Pearson has written a memo, included as Attachment B, which describes the philosophical reasons that favor orienting the defining and support units for a meniscus mirror along the coordinate directions of a spherical coordinate system, which results in the "axial" supports being applied normal to the mirror back surface as in the Gemini design. The axial and lateral supports are in fact orthogonal, and do not cross couple.

One of the principal advantages of aligning the axial defining mechanisms normal to the optical surface is that mirror movement caused by the lateral support produces rotation about the center of curvature instead of a lateral translation. This is an important consideration in maintenance of optical alignment as the telescope changes zenith angle.

Another consideration is to avoid bonding 120 Invar pads to the back of the mirror. The Gemini axial support is designed to be under compression at all times during operation; therefore it does not require the mechanisms to be bonded to the mirror. For a support that is not normal to the mirror surface, there will be a lateral force component at the interface unless wedge-shaped pads are bonded onto the back of the mirror. Use of such pads adds cost, complexity, and potential for error, and complicates procedures when the mirror is removed for recoating.

Except for telescope alignment issues and the need for pads on the back of the mirror, our studies have shown that the mirror support could be made to work adequately either using supports oriented with a spherical coordinate system ("normal") or with a Cartesian coordinate system ("parallel"). The parallel system can be optimized to yield a residual gravity distortion that is equal to the normal system, and their active optics correction capabilities are also about equal. However, there is a slight difference in the interaction with the air pressure support.

If the air pressure varies over periods of less than two or three minutes, the active optics system cannot correct any resulting deformations. To first order, if the support forces act normal to the mirror surface, as does the air pressure, the only effect of air pressure variation will be a change in print-through. The parallel support will change both print-through and global figure. However, the differences are small. Our analysis shows that under a 5 % air pressure change the support normal to the mirror surface has 20% better performance than the support parallel to the optical axis (31 nm vs 37 nm surface error without active optics correction).

Therefore, to ease alignment problems, to avoid having to bond 120 Invar pads to the glass, and to improve the interaction with the air pressure support, the support forces should be applied normal to the mirror surface.

V. Air Pressure Support or Load Spreaders

To minimize support print-through the Gemini design uses a controlled air pressure to carry 80% of the mirror weight at Zenith, with the air pressure decreasing with Zenith angle to ensure the load carried by the axial support mechanisms is invariant with Zenith angle over the operating range of the telescopes. This allows the print-through from the 20% of the mirror weight carried on the axial support mechanisms (about 10 nm RMS) to be polished out at Zenith pointing, and it will not return at other Zenith angles.

However, the PDR Committee report recommends,

"The use of load spreaders instead of an airbag support to reduce actuator "printthrough" to acceptable levels should be investigated."

Engineers at REOSC have also suggested the use of load spreaders, and load spreaders are being used by some of the other large telescope projects.

The ESO VLT design uses a load spreading tripod on each axial support. The tripod legs are attached to 450 Invar pads bonded to the back of the mirror. These legs apply lateral as well as axial forces in carefully designed proportions, thus reducing the support print-through to approximately the 10 nm RMS level. If this print-through is polished out at the Zenith, it will return in inverse at increasing Zenith angles. For example, at $Z = 30^\circ$ the print-through would be about 5 nm RMS.

Some other mirror support designs, for example, the Columbus Project primary mirror support, use triangular plates to spread the load from each support onto three pads. In the Columbus design the pads are bonded to the back of the mirror, because they also provide the lateral support of the borosilicate mirrors.

Jacques Paseri of REOSC has proposed the use of load spreaders in the form of a two-level whiffletree. Each load spreader would be "H" shaped, with two pivoting beams on top of a central beam that would in turn pivot on the support mechanism. Each load spreader would have four pads supporting the mirror.

The Gemini Project has considered these and other types of load spreaders, and has decided the most practical type to consider is a three-pad spreader consisting of three cantilever beams 120° apart, as shown in Figure 3. This choice is driven by three design goals: (1) to avoid bonding pads to the back of the mirror; (2) to maintain a stiff load path from the mirror to the hydraulic cylinders in the support mechanisms; and (3) to minimize the mass of the load spreaders.

Preliminary design layouts showed that the most even spacing of the support pads would result from a load spreader arm length of approximately 250-300 mm. However, to maintain the required stiffness of about 18 N/ μm , the arms would have to be thick and heavy. Since the deflection under load varies as the length cubed, the arms were shortened to 200 mm, allowing the dimensions shown in Figure 3 for a load spreader made of steel. If the load spreader were made of Invar, the wall thickness (and the weight) would be about 45% higher.

Finite-element analysis was conducted to determine the print-through on the mirror resulting from the use of these load spreaders. Eight different arrangements of the load spreaders were studied. The best arrangement was as shown in Figure 4. The resulting surface error is 18 nm RMS. It is believed that further optimization of the support locations and load spreader orientations could reduce this error by about 20%.

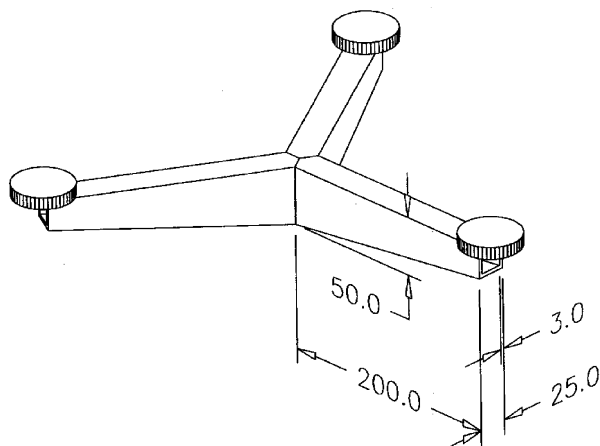


Figure 3. The proposed load spreader design.

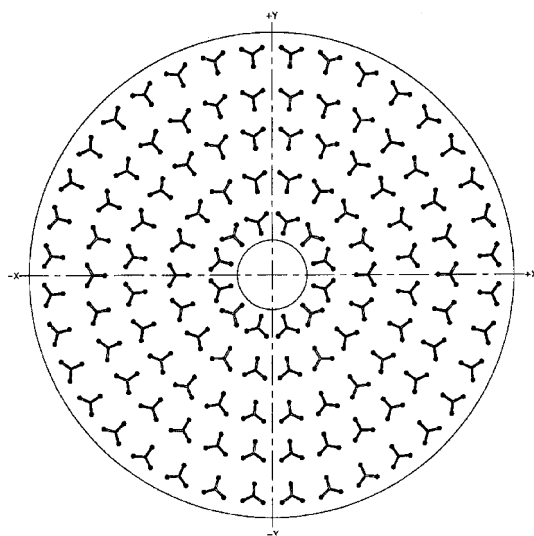


Figure 4. Locations and orientations of load spreaders.

Note that if this print-through were polished out at the zenith, it would reappear at other elevations as a function of increasing zenith angle:

$$A = A_0(1 - \cos Z)$$

where:

A = amplitude of print-through

A_0 = amplitude calculated for zenith-pointing gravity deflection

Z = zenith angle

The map of print-through deflections determined by finite-element analysis has been converted to an interferogram file and input to Code V, and diffraction calculations have been made to determine the effect on the encircled energy in the image at several wavelengths. These results

are shown in Table 2. Three-dimensional plots of the point spread functions produced by this mirror surface, at each wavelength, are shown in Figures 5 through 9.

Table 2. Increase in encircled energy diameters produced by load spreader print-through.

Wavelength	Encircled Energy Diameter Increase, Calculated by Quadrature Subtraction (arcsec)	
	50%	85%
310	0.0078	0.2173
550	0.0066	0.0968
800	0.0064	0.0409

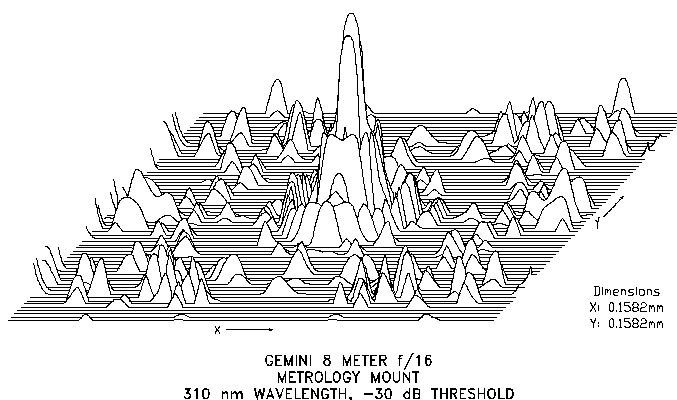


Figure 5. A logarithmic plot of the point spread function produced by the mirror supported on the load spreaders, at a wavelength of 310 nm.

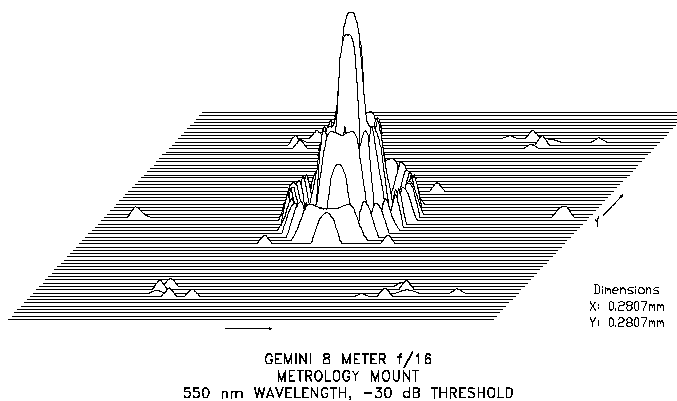


Figure 6. A logarithmic plot of the point spread function produced by the mirror supported on the load spreaders, at a wavelength of 550 nm.

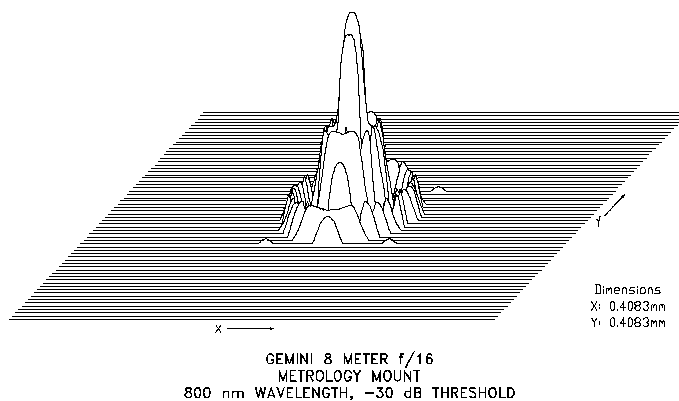


Figure 7. A logarithmic plot of the point spread function produced by the mirror supported on the load spreaders, at a wavelength of 800 nm.

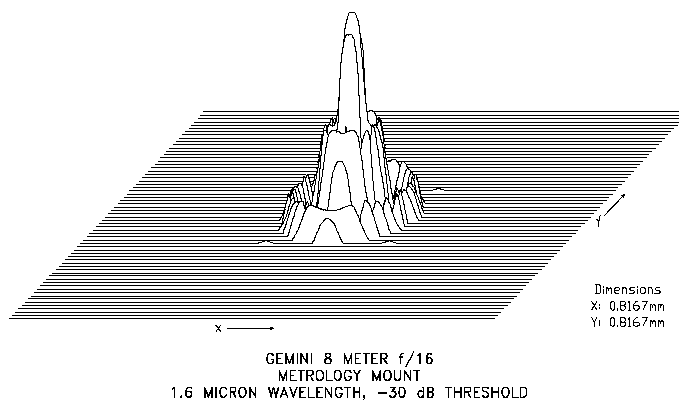


Figure 8. A logarithmic plot of the point spread function produced by the mirror supported on the load spreaders, at a wavelength of 1.6 microns.

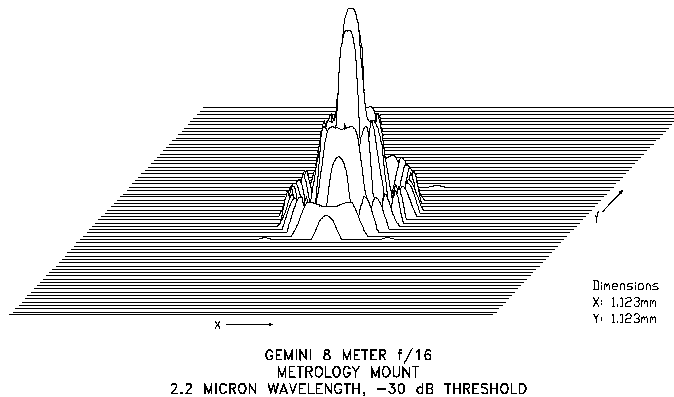


Figure 9. A logarithmic plot of the point spread function produced by the mirror supported on the load spreaders, at a wavelength of 2.2 microns.

The load spreaders have the following advantages:

1. Use of load spreaders would eliminate the need for the air pressure support; however, some form of simple seal would still be needed around the inside and outside diameters of the mirror to prevent moisture condensation on the radiation plates of the thermal management system.
2. Use of the load spreaders would save part of the cost of the Air Pressure Support System option at REOSC. The cost savings would be offset by other costs that would be incurred as a result of the design change (see item 6, below).

The load spreaders have several disadvantages:

1. Each load spreader would weigh about 18-20 newtons (about 4 pounds) if made of steel, and about 26-29 newtons if made of Invar. When the telescope points away from the zenith, the lateral component of this weight would apply a side load to the mirror, producing figure errors requiring active optics correction. When the telescope is pointed to the horizon, for example to clean the mirrors, the load spreaders might shift laterally, introducing additional errors.
2. The weight of the load spreaders would complicate the design of the flexures that provide the lateral compliance needed to compensate for relative expansion of the mirror cell. The flexures could easily be damaged if each supported a large, relatively heavy load spreader.
3. Relative thermal expansion between the load spreader and mirror would also be a problem. Relative expansion of the spreader would introduce a bump or dimple over the support that could not be alleviated by active optics. To prevent this, the load spreaders could be made of zero-expansion material, or could be made from two dissimilar materials in a carefully designed combination that compensated for the relative expansion of each. In either case, the cost would be fairly high.
4. The load spreaders would interfere with the radiation plates of the thermal management system. Even if more room were provided between the mirror and cell to avoid a physical interference, the load spreaders would block the heat transfer at 120 locations on the mirror.
5. Replacement of a mirror support mechanism would be complicated by the fact that the load spreader could not be pulled down through the mechanism mounting flange.

6. Changing to the load spreader approach would require reoptimization of the support locations, recalculation of all the active optics influence functions, adjustment of the cell structural design, redesign of the radiation plates, plus careful design of the load spreaders themselves.

The air pressure support has a number of advantages:

1. The relative accuracy requirements for the load cells can be relaxed. If load spreaders were used, the full mirror weight would rest on the load cells, and the small active optics force adjustments would be measured relative to that total force. With the air pressure support, the operating range of the load cells is limited to 20% of the mirror weight, allowing lower relative accuracy and repeatability. The load cells would still need to survive application of the full mirror weight, but would only need to be repeatable and linear over the smaller range.
2. The air pressure support maintains a total force on the axial support mechanisms that is invariant with zenith angle. As described above, this allows print-through to be polished out at the zenith and it does not reappear at other zenith angles.
3. The seals of the air pressure support prevent condensation on the thermal management system radiation plate.

Conclusion:

The air pressure support offers better performance than load spreaders; this is particularly noticeable at shorter wavelengths. We believe the cost to design, fabricate, assemble and install the load spreaders will be comparable to the cost to design, fabricate and install the air pressure support. Therefore, the air pressure support is the better choice.

VI. Active Optics Actuators Around the Outer Edge

The original Gemini support design includes 72 active actuators around the outer edge, out of a total of 192 actuators. These edge actuators were intended to serve several purposes: (1) to provide a means for correcting force components normal to the mirror surface produced by alignment errors in the lateral supports; (2) to provide a means for correcting the effect of any force errors introduced by the outer air pressure seal; (3) to help correct rotationally symmetric aberration terms, such as spherical aberration, that are difficult to produce because of steep slopes required at the edge of the aperture.

However, other large telescopes projects have not seen the need for actuators around the edge, and these actuators are not included in the REOSC metrology mount. One of the recommendations of the PDR Committee was:

"The need for the peripheral ring of 72 axial actuators should be justified."

A number of finite-element cases have been run to determine the active optics performance penalty to be paid for giving up these actuators. These cases are described below, and the results are summarized in Table 3.

Case 1. This case models the effect of tilting the primary mirror by 15 arcsec relative to the mirror cell, to maintain alignment with the Cassegrain Rotator axis as the telescope moves in zenith angle from 0 to 75°. This shifts the angle of the lateral supports, and produces force components perpendicular to the mirror surface ranging up to 8N.

Case 2. This case models an unintended force change at the outer air pressure seal of 5 N/m.

Case 3. Case 3 models a force error of 10 newtons, perpendicular to the mirror surface, at one of the lateral supports. This type of error could be caused by misalignment of one of the lateral support units, for example.

Case 4. This case models a moment error of one newton-meter applied to the mirror outer edge, which could be caused by friction in the lateral support linkage joints.

Case 5. Case 5 models the application of active forces to change the hyperboloid mirror figure to a paraboloid. This is accomplished by combining Zernike spherical aberration with Zernike focus to produce a figure change that approximately matches a mirror bending mode.

Case 6. Case 6 measures the ability of the active optics system to compensate for gravity-induced deflection of the secondary mirror, in this case at a zenith angle of 45°.

Case 7. This case models the predicted distortion of the mirror that would occur because of variations in the coefficient of thermal expansion of the material. The model assumes the mirror is figured in the optics shop at 20° C, and is then used at a temperature of -5° C.

Case 8. Case 8 is an extreme case that represents a failure mode in which one actuator goes to its force limit (400 N) and stays there. (No mechanism has actually been proposed that could cause such a failure.) In this case, the failed actuator is located at about a 60% radius. The active optics system is used to correct the mirror figure resulting from this malfunction.

Table 3. A comparison of active optics performance with 192 versus 120 active actuators.

Case Number	Figure Error Before Active Optics Correction (nm RMS)	Residual Figure Error After Active Optics Correction, and Required Maximum Force			
		192 Actuators		120 Actuators	
		(nm RMS)	Force (N)	(nm RMS)	Force (N)
1	96	1.6	3	3.2	4
2	135	0.1	3	0.9	6
3	50	0	10	0.3	15
4	2	0.03	1.7	0.09	2.3
5	200	4	12	4	20
6	13	2	4	2	4
7	660	4	33	7	40
8	2255	6.4	204	7.5	278

In general, the residual figure error is higher with only 120 actuators, and the maximum force is larger. However, the residual errors are small for either 192 or 120 actuators, and in all cases except case 8 (an extreme failure mode) the corrective forces are small, and they are well within the force budget for the active optics system, which is shown in Table 4. There is still force margin left, even without the edge active actuators.

Table 4. Force budget for GEMINI active optics system

Error Source	Maximum Active Force Required Using Either 192 or 120 Actuators (N)			
	Independent Factors (added in quadrature)		Dependent Factors (added algebraically)	
	192	120	192	120
Nominal Support Design			20	25
Axial Support Errors				
Crosstalk Errors (orthog. forces & moments)	20	25		
Angle Errors	45	55		
Position Errors	13	18		
Lateral Support Errors				
Force Errors	17	25		
Crosstalk Errors (orthog. forces & moments)	20	30		
Angle Errors	70	100		
Position Errors	40	50		
Air Pressure Support Errors				
Pressure Errors	1	1		
Seal Force Errors	60	140		
M1 Cell Thermal Expansion	10	14		
Primary Mirror				
Decenter	23	30		
Polishing	100	100		
Thermal Effects				
Delta CTE			33	40
Axial Temperature Gradient			45	50
Other Non-uniform Temperature Patterns	30	40		
Steady Wind	24	25		
Change Mirror Figure From Cass. to R-C.			12	20
Secondary Mirror				
Gravity Sag (up to $Z = 75^\circ$)			10	10
Polishing errors	100	100		
Thermal Distortion: Non-uniform Temp.	10	10		
Subtotal: RSS of Independent Effects	189	247		
Subtotal: Sum of Dependent Effects			120	145
Total Force Requirements: RSS of Subtotals			224	286
Force Budget Per Actuator			386	386
Residual Budget for Unidentified Factors (quadrature subtraction)			314	259

VII. Conclusions

As a result of these studies, Gemini Project staff have reached the following conclusions:

1. The Gemini pattern of 120 supports should not be changed to match the ESO pattern of 150 supports. The ESO pattern is not well optimized for the Gemini mirror. The REOSC option to change the support pattern of the metrology mount should be exercised.
2. The support forces should be oriented normal to the mirror surface, as in the original Gemini design. Therefore, the supports in the REOSC metrology mount should also be oriented normal to the mirror surface.
3. The air pressure support has advantages over the use of load spreaders. The REOSC option to implement a matching air pressure support in the metrology mount should be exercised.
4. The active optics actuators at the outer edge of the mirror would be beneficial, but the error budget and active optics force budget can still be met without them. The REOSC option for installation of these actuators should not be exercised, and they will be deleted from the mirror cell design.

VIII. Acknowledgements

The author would like to acknowledge the contributions of Myung Cho, who did the finite-element analysis for this report, John Roberts, who performed the optical analysis and prepared the related figures, and Dale Circle, who prepared the drawings shown in several of the figures..

ATTACHMENT A

DISCUSSION OF THE PROBLEMS INTRODUCED IF THE METROLOGY MOUNT DOES NOT MATCH THE TELESCOPE MIRROR SUPPORT DESIGN

Larry Stepp

As a cost saving measure, REOSC proposed use of a metrology mount based on the one used for the VLT, with the addition of 46 cm diameter load spreading pads on each of the 150 support locations. Their calculations showed that this mount would only distort the mirror figure by 4.3 nm RMS. In other words, if the mirror appeared perfect when tested on this support, there would in fact be stresses present in the material that would distort the mirror figure by 4.3 nm RMS when it was moved to a different support.

The Gemini support design will introduce about 10 nm RMS of print-through, as shown in Figure A1, below. Our plan is to polish out this print-through at zenith pointing in the optics shop, then control the air pressure support to ensure it does not reappear at any other zenith angle. To accomplish this, the mirror must be tested in the optics shop on a metrology mount that matches the mirror support used in the telescope.

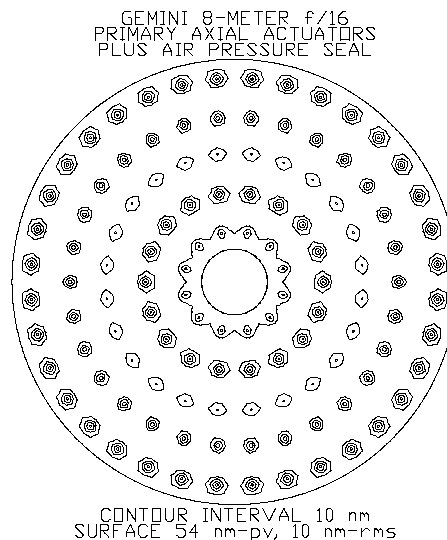


Figure A1. The print-through deformation of the optical surface of the primary mirror caused by the Gemini Support System, with 80% of the weight carried by the Air Pressure Support (before compensation).

If the metrology mount does not match the telescope mirror support, the figure the mirror exhibits in the telescope would differ from the figure tested in the optics shop by the summation of the Gemini print-through plus the inverse of the REOSC print-through. These actual print-through effects may differ somewhat from those calculated by finite-element analysis, because the loading conditions may be slightly different in the actual support systems than the conditions assumed for the analysis. Therefore, it would be risky to try to compensate for this combined print-through by polishing dimples into the mirror surface at 120 locations, based solely on finite-element calculations.

The effect of the print-through shown in Figure A1 on the image point spread function has been calculated using Code V. The finite-element results have been converted into a 512 x 512 Code V interferogram file, and a diffraction calculation has been done to determine the effects on energy concentration. The following table lists the increases in encircled energy diameter that would be produced by the calculated Gemini print-through. Note that the effects are more pronounced at shorter wavelengths, and are larger for 85% encircled energy than for 50%.

Table A1. Increase in encircled energy produced by the support print-through shown in Figure A1.

Wavelength (nm)	Quadrature Increase in Encircled Energy Diameter (arcsec)	
	50%	85%
310	0.0041	0.0614
550	0.0040	0.0235
800	0.0039	0.0221
1600	0.0039	0.0213
2200	0.0039	0.0213

Figures A2 through A6 show the encircled energy as a function of image diameter for the nominal system and for images produced by the surface in Figure A1, for five different wavelengths. It can be seen from examination of the plots that, as expected, the angle through which the energy is diffracted increases with wavelength, while the amount of energy diffracted out of the central core varies as the inverse of the square of the wavelength.

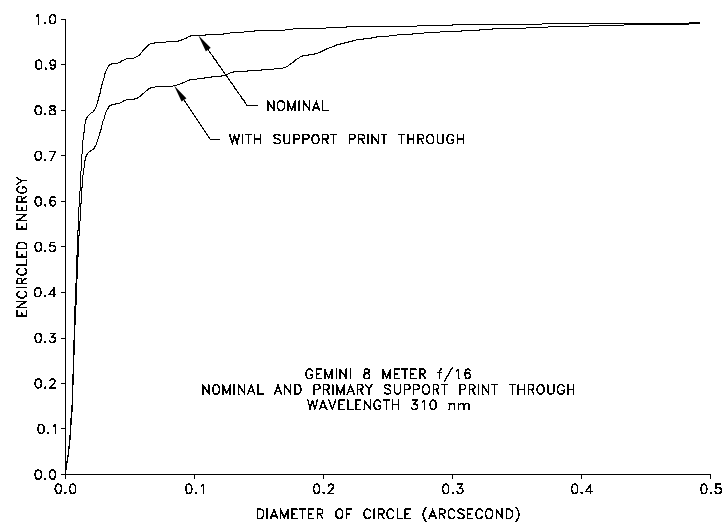


Figure A2. Encircled energy as a function of image diameter, at a wavelength of 310 nm.

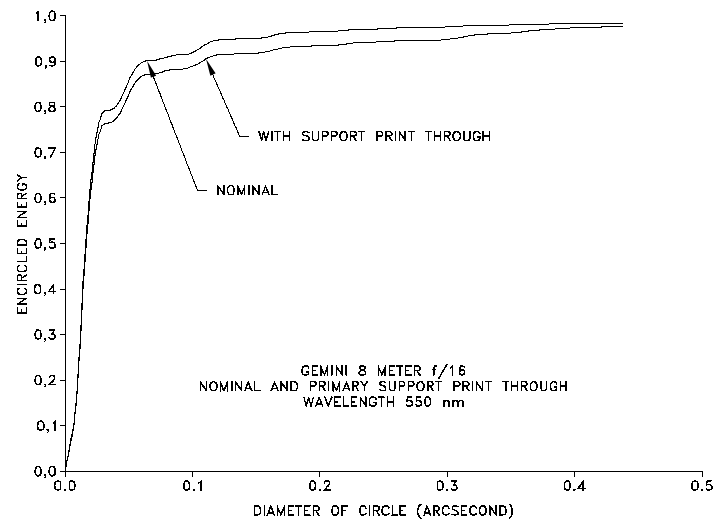


Figure A2. Encircled energy as a function of image diameter, at a wavelength of 550 nm.

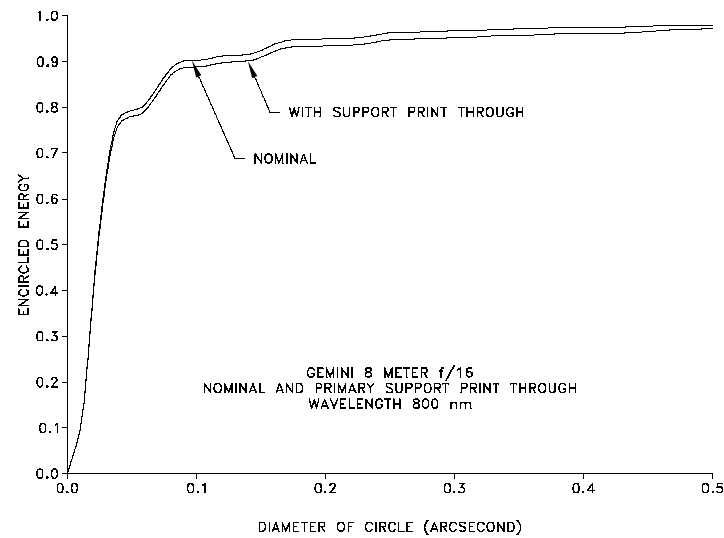


Figure A2. Encircled energy as a function of image diameter, at a wavelength of 800 nm.

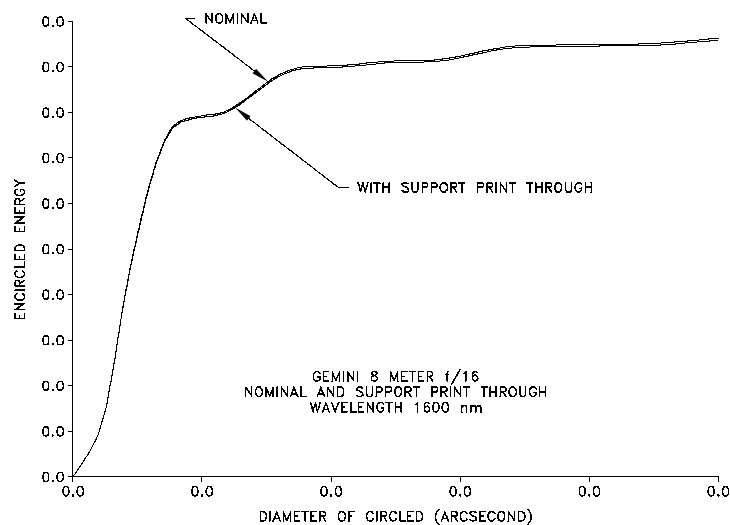
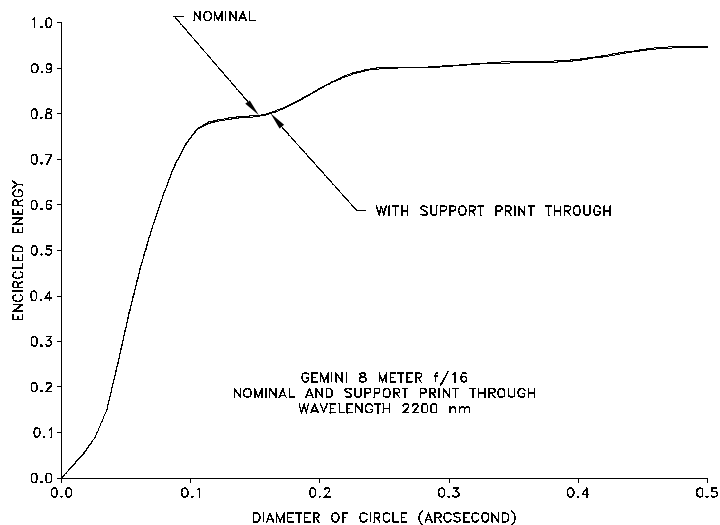


Figure A2. Encircled energy as a function of image diameter, at a wavelength of



1600 nm.

Figure A2. Encircled energy as a function of image diameter, at a wavelength of 2200 nm.

Because the print-through pattern in Figure A1 is very regular, there is a potential for problems with satellite images. Figures A7 through A11 show the point spread functions produced by the print-through surface at different wavelengths, and satellite images are clearly present. Each plot is plotted on a logarithmic scale, with the threshold of detectability set at -35 dB (one part in 3,162).

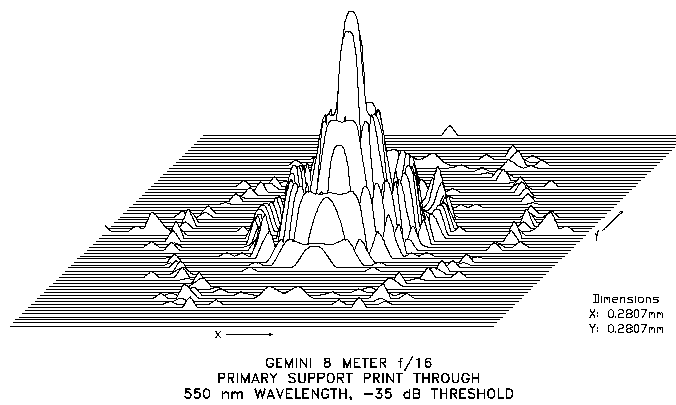
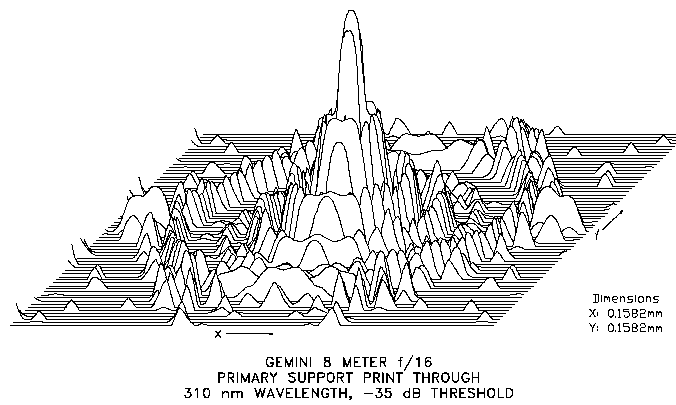


Figure A7. A logarithmic plot of the point spread function produced by the surface shown in Figure A1, at a wavelength of 310 nm. Width of plot is .25 arcsec.

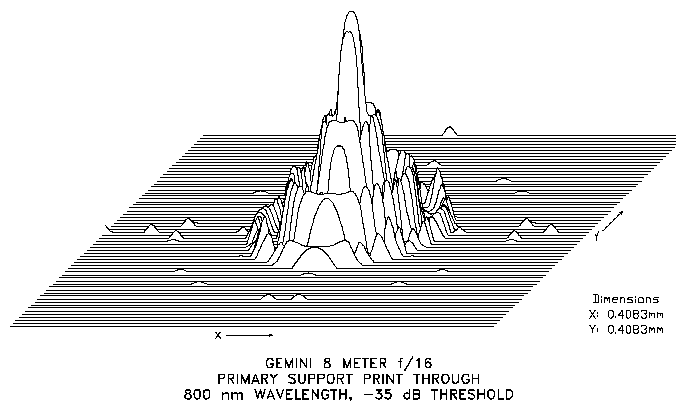


Figure A8. A logarithmic plot of the point spread function produced by the surface shown in Figure A1, at a wavelength of 550 nm. Width of plot is .45 arcsec.

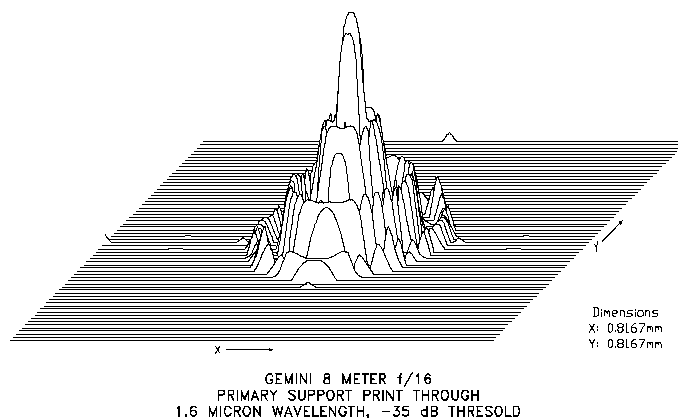
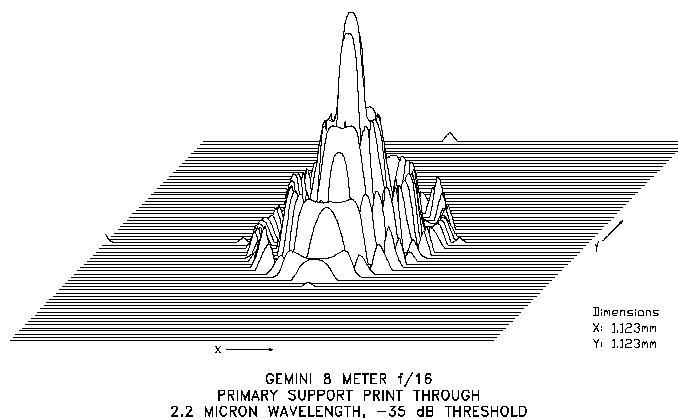


Figure A9. A logarithmic plot of the point spread function produced by the surface



shown in Figure A1, at a wavelength of 800 nm. Width of plot is .66 arcsec.

Figure A10. A logarithmic plot of the point spread function produced by the surface shown in Figure A1, at a wavelength of 1600 nm. Width of plot is 1.32 arcsec.

Figure A11. A logarithmic plot of the point spread function produced by the surface shown in Figure A1, at a wavelength of 2200 nm. Width of plot is 1.81 arcsec.

$$\frac{I_a(r)}{I_p(0)} \leq 1.267 \times 10^{-5} \left(\frac{\lambda}{r} \right)^3$$

Paul Hickson and Gordon A. H. Walker¹ have developed a specification for allowable satellite image intensities based on noise detectability after background subtraction. For an 8-meter telescope, this specification requires:

where: $I_a(r)$ = intensity of satellite image at radius r
 $I_n(0)$ = central intensity of image
 λ = wavelength in microns
 r = radius position in arc seconds

The intensity of the satellite images has been compared to the specification at each of the five wavelengths. Table A2 lists the range of image radii over which the specification is exceeded, for each wavelength. The maximum range of radii considered in the analysis was from 0.1 to 4 arcseconds.

Table A2. Range of image radii for which the satellite image intensity specification is exceeded, for five wavelengths.

Wavelength (nm)	Range of Image Radii over which Criterion is Exceeded (arcsec)	Intensity Data for Worst Out-of-Spec. Points		
		Calculated Intensity Ratio	Specified Intensity Ratio	Radius of Out-of-Spec. Point (arcsec)
310	0.10-0.26	0.00195	0.00036	0.10
500	0.16-0.21	0.00067	0.00037	0.18
800	None	None	None	None
1600	None	None	None	None
2200	1.69-2.62	0.00003	0.00001	2.62

The results presented in this appendix are optimistic, because they do not include the deformations caused by the REOSC metrology mount, and they are for calculated print-through only. The results are optimistic for another reason, as well. The Gemini polishing specification allows active optics correction of the mirror figure in the optics shop. While the REOSC metrology mount does have active optics capabilities, the high-frequency residuals introduced by its active optics correction would be different than those introduced by the Gemini active optics system. Therefore, the global figure might be adequately corrected, but the high frequency effects might not meet the Gemini encircled energy specifications.

Acknowledgments

The author would like to acknowledge the contributions of Myung Cho, who did the finite-element analysis for this report, and John Roberts, who performed the optical analysis and prepared the related figures.

References

1. Proposed Image Quality Specification for the Gemini Telescopes, Paul Hickson and Gordon A. H. Walker, June 3, 1992.

ATTACHMENT B

Spherical Coordinates and the Meniscus Mirror (Orthogonality)

Earl Pearson

The geometry of the meniscus mirror should be thought of as a section of a spherical shell. The mirror surface has a radius of curvature (twice the focal length) and the corresponding center of curvature is the center of the sphere. The "back" surface of the mirror has the same center of curvature but the radius is more than the front surface by the thickness of the mirror (20 cm for our case). The edges of the mirror are then formed by the right circular cone whose vertex is the center of the sphere and whose diameter corresponds to the mirror diameter at the mirror surface. However, while the back and edges can maintain these shapes, the front (mirror) surface has a small departure from the sphere for optical reasons. The maximum departure is 0.032 cm from the best fitting sphere (0.16% of the thickness).

We can now define a coordinate system to our mirror. Let r be the radius measured from the center of the sphere. The line connecting the vertex of the mirror to the center of the sphere is the reference (zero) for the angle ϕ . Finally, the angle θ is measured from an arbitrary direction as indicated in the figure below. Coordinate surfaces are defined by r , ϕ and θ of constant values. Thus, the mirror and back surfaces are both $r = \text{constant}$ surfaces. The outer edge is an $\phi = \text{constant}$ surface. The $\theta = \text{constant}$ surfaces are interior to the mirror material. If the mirror were sliced exactly in half across a "diameter" of the mirror surface, then the cross section of the mirror would be a θ surface.

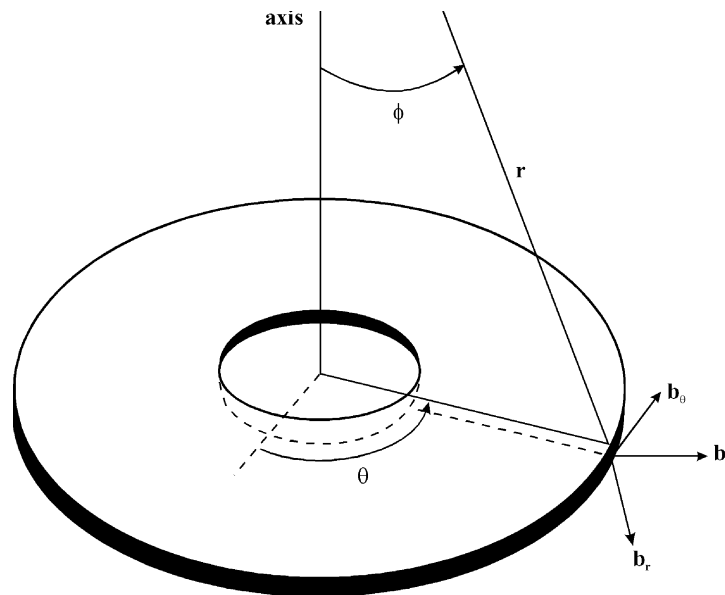


Figure B-1. The mirror as a spherical shell and the spherical coordinates r , ϕ and θ

Once we have these coordinate surfaces, we can define unit base vectors that are perpendicular to these surfaces. Thus \mathbf{b}_r is perpendicular to an r surface, \mathbf{b}_ϕ is perpendicular to a ϕ surface and \mathbf{b}_θ is perpendicular to a θ surface. These are also illustrated in Figure B-1. These base vectors are all mutually perpendicular to each other (orthogonal). This means that small forces or displacements in one of these directions is not coupled to the other two.

How does this affect our mirror in practice? Let there be a series of "pinned-end" bars in the \mathbf{b}_r direction on the back surface (an r surface) of the mirror. These are illustrated in Figure B-2(a). This is just one ϕ surface (a 2-D slice through the mirror). For *small* values of $\Delta\theta$ or $\Delta\phi$ the mirror would be essentially unconstrained. It would, however, be constrained in the r direction. Thus the spherical mirror would move along the original spherical surface instead of perpendicular to the optical axis. This has advantages for optical alignment, etc. In Figure B-2(b), we have pinned-end bars on the outer edge (a ϕ surface) in the \mathbf{b}_ϕ direction. These would allow *small* displacements in the θ and r directions but not in ϕ . Finally, in Figure B-2(c) are the θ constraints. Small movements of ϕ and r are allowed while $\Delta\theta$ is not.

The support system should be thought of on the basis of this orthogonal coordinate system. The air pressure on the back surface always produces forces normal to that surface. These forces add or subtract from the "r constraints" but do not affect any change in the θ or ϕ constraints. If the perpendicular bars were replaced with bars that were all aligned with the optic axis, this would no longer be true. We would have a coupling of the force systems. If the ϕ constraints were replaced by bars perpendicular to the optic axis, again there would be coupling between the two supports. If small displacements were associated with constraints, then forces would develop that could distort the mirror. Coupling should be avoided when possible since an error in one mechanism would then automatically produce an error in the other system.

Figure B-2. Example supports (constraints) in the coordinate base vector directions.

